Magnetic behaviour of $(RPd_3)_8Al$ (R = Gd to Yb) and $(CePd_3)_8Al_{0.5}Zn_{0.5}$

2002 J. Phys.: Condens. Matter 14 11795

(http://iopscience.iop.org/0953-8984/14/45/321)

INSTITUTE OF PHYSICS PUBLISHING JOURNAL OF PHYSICS: CONDENSED MATTER

J. Phys.: Condens. Matter **14** (2002) 11795–11808 PII: S0953-8984(02)52194-9

Magnetic behaviour of $(RPd_3)_8Al$ (R = Gd to Yb) and $(CePd_3)_8Al_{0.5}Zn_{0.5}$

Surjeet Singh and S K Dhar[1]

CMP&MS, TIFR, Homi Bhabha Road, Mumbai 400 005, India

E-mail: sudesh@tifr.res.in (S K Dhar)

Received 9 August 2002
Published 1 November 2002
Online at stacks.iop.org/JPhysCM/14/11795

Abstract

We have synthesized new compounds with the composition $(RPd_3)_8Al$ (R = La, Gd, Tb, Dy, Ho, Er, Tm, Yb and Y) and $(CePd_3)_8Zn_{0.5}Al_{0.5}$. These compounds have cubic symmetry and are iso-structural to $(CePd_3)_8Al$, reported earlier in the literature. Compounds with R = Gd, Tb, Dy and Ho order magnetically above 1.6 K and their transition temperatures are greater than those of the corresponding RPd_3 analogues. $(TbPd_3)_8Al$ shows an appreciable thermomagnetic irreversibility in its magnetization measured in low fields below the Néel temperature T_N. The peak position in its ac susceptibility is frequency independent (1–999 Hz), which shows that the irreversibility is not driven by spin-glass-type freezing of the Tb moments. To a lesser extent, Dy and Ho compounds also exhibit irreversibility in their low-field magnetization below the Néel temperature while it is absent in the Gd compound. Metamagnetic transitions are seen in the isothermal magnetizations of Tb, Dy and Ho compounds below T_N while such a feature is absent in the Gd compound. Resistivity mimima are seen for R = Gd, Tb, Dy and Ho and these arise most likely from the critical scattering above T_N. The heat capacity data corroborate the long-range magnetic order in these four compounds and indicate a relatively low crystal electric field splitting. The substitution of Al with Zn by as much as 50% in the parent dense Kondo lattice antiferromagnet $(CePd_3)_8Al$ expands the lattice marginally. The resistivity of $(CePd_3)_8Zn_{0.5}Al_{0.5}$ shows Kondo behaviour and exhibits a peak around 50 K. The corresponding feature in $(CePd_3)_8Al$ occurs near 10 K. T_N increases marginally by 0.2 K due to the Zn substitution.

1. Introduction

Recently, Gordon *et al* [1, 2] reported the synthesis of $(CePd_3)_8T$ (T = Ga, Sn, In, Pb, Sb and Bi) compounds, which form in a cubic superstructure closely related to the cubic $AuCu_3$-

[1] Author to whom any correspondence should be addressed.

type structure of the parent $CePd_3$. The bigger p-block, T atom occupies the body-centred position of the unit cell of $CePd_3$ and pushes the Pd atoms outward from the faces of the cube such that a T atom cannot be accommodated in the adjacent cells within a distance (measured between the centres of the unit cells) less than or equal to $a\sqrt{3}$, where a is the lattice parameter of the $CePd_3$ unit cell. The crystal symmetry and the space group of $(CePd_3)_8T$ remain the same as that of the parent $CePd_3$ but with a lattice parameter a slightly larger than twice that of $CePd_3$. While Ce remains coordinated by 12 Pd atoms in the superstructure, the Ce–Ce separation is increased by 2–3% over its value in $CePd_3$. In a later study it was found that the superstructure is also formed with T = Ge and Al [3, 4]. $(CePd_3)_8T$ compounds order magnetically below 10 K, exhibiting heavy-fermion-like enhanced low temperature electronic specific heat coefficient γ [3–6]. Mitra *et al* [7] explored the superstructure formation for other R atoms and obtained iso-structural single-phase compounds $(RPd_3)_8T$ for R = La, Pr, Nd, Sm, Gd, Tb, Y, Dy, Er and Lu and T = Ga and Ge. First-order antiferromagnetic ordering and metamagnetic transitions were observed in $(TbPd_3)_8T$ (T = Ga and Ge) [7]. In the present work we have investigated the formation of analogous $(RPd_3)_8Al$ compounds. We find that indeed iso-structural compounds $(RPd_3)_8Al$ for (R = La, Gd, Tb, Dy, Ho, Y, Er, Tm and Yb) exist with lattice parameters similar in magnitude to those of corresponding Ga and Ge compounds. Typically, the magnetic transition temperatures of $(RPd_3)_8Al$ compounds are higher than those of the corresponding RPd_3.

Gordon *et al* [4] also tried making $(CePd_3)_8Zn$ in a closed tantalum crucible. Though the powder x-ray patterns showed the presence of superstructure, the sample was not homogeneous and its stoichiometry was uncertain. In the present work we have successfully prepared single-phase $(CePd_3)_8Zn_{0.5}Al_{0.5}$, which shows that Al can be substituted with Zn at least up to 50%. The magnetic properties of the Zn-substituted compound are also described in this paper.

2. Experimental details

The alloys $(RPd_3)_8Al$ for R = La, Ce, Gd, Tb, Dy, Ho, Y, Er, Tm and Yb and $(CePd_3)_8Zn_{0.5}Al_{0.5}$ were made by the standard technique of arc melting in an inert atmosphere of argon. First weighed amounts of R and Pd were melted in an inert atmosphere of high purity argon gas to form RPd_3; the weight loss in this process was about 0.5% in all cases. Then a weighed amount of Al was melted with the RPd_3 button in which the weight loss was negligible. The buttons were flipped over and re-melted several times to ensure homogenization. The samples were then sealed in an evacuated quartz tube and heat-treated at 800–900 °C for 14 days. To make the Yb compound the method of preparation is somewhat more involved due to the volatile nature of Yb. First a weighed amount of Pd foil was moulded in the form of a cup with a fitting lid. The cup was then inserted in a stainless steel die, whose diameter approximately matches the diameter of the cup; Yb pieces (an excess of 3% was taken) are then poured into the cup from the top and the cup is closed with the Pd lid. It was then pressed at moderate pressure to form a pellet and there was no weight loss in the process. The pellet was melted in the arc furnace in flowing argon of high purity; the weight loss at the end of the third melt was about 5% of the total Yb weight. The $YbPd_3$ button was then melted with the weighed amount of Al and there was practically no weight loss in this melting. Our Yb sample is therefore slightly sub-stoichiometric in Yb. To make the alloy of $(CePd_3)_8Zn_{0.5}Al_{0.5}$ we first made a $(CePd_3)_8Al_{0.5}$ button using the same procedure as for $(RPd_3)_8Al$. Keeping in mind the low heat of vaporization of Zn, a slight excess of Zn was taken to compensate for any weight loss during melting. After four arc-melts we found that there was practically no weight loss and our sample therefore is slightly hyper-stoichiometric in Zn. The Zn sample was not subjected to any heat treatment. The phase purity of the samples was checked by powder x-ray

Table 1. The lattice parameter (a), effective paramagnetic moment (μ_{eff}), paramagnetic Curie temperature (θ_P) and magnetic transition temperature obtained from heat capacity data (T_N) of $(RPd_3)_8Al$ and $(CePd_3)_8Zn_{0.5}Al_{0.5}$. The T_N of RPd_3 compounds is taken from [16].

Sample	a (Å)	μ_{eff} (μ_B)	θ_p (K)	T_N (K)	T_N (RPd_3) (K)
$(LaPd_3)_8Al$	8.455	—	—	—	—
$(CePd_3)_8Al$	8.393	—	—	4.4	—
$(GdPd_3)_8Al$	8.272	8.60	−10.0	10.0	7.5
$(TbPd_3)_8Al$	8.233	9.98	7.4	5.3	2.5
$(YPd_3)_8Al$	8.223	—	—	—	—
$(DyPd_3)_8Al$	8.220	10.6	−0.7	4.0	1.5
$(HoPd_3)_8Al$	8.202	10.3	3.4	2.6	—
$(ErPd_3)_8Al$	8.194	9.62	−1.3	—	<3
$(TmPd_3)_8Al$	8.159	7.53	1.4	—	0.2
$(YbPd_3)_8Al$	8.140	4.41	4.3	—	0.18
$(CePd_3)_8Zn_{0.5}Al_{0.5}$	8.404	2.56	−27.0	4.6	—

diffraction. The resistivity of the samples was measured by the four-probe dc method using typically a current of 30 mA. The heat capacity was measured by using the semi-adiabatic, heat pulse method. Magnetization as a function of temperature and field was recorded on the VSM (Oxford Instruments) and SQUID (Quantum Design) magnetometers.

3. Experimental results

3.1. $(RPd_3)_8Al$ (R = La, Gd, Tb, Dy, Ho, Er, Tm, Yb and Y)

The powder x-ray diffraction patterns of $(GdPd_3)_8Al$ and $(CePd_3)_8Zn_{0.5}Al_{0.5}$ taken with Cu Kα radiation, together with Rietveld fitting, are shown in figure 1 as typical examples. The diffraction patterns of the other compounds look similar. The high-intensity peaks are characteristic of the diffraction pattern from the RPd_3 lattice. Additional low-intensity 'satellite peaks', indicated by asterisks, arise due to the formation of cubic superstructure in the $(RPd_3)_8Al$ lattice. Figure 2 shows a picture of a conventional unit cell of $(RPd_3)_8Al$; the displacement of the Pd atoms from their normal positions in RPd_3 is clearly evident. Rietveld refinement revealed that the distortion of the Pd polyhedra (and the resulting intensity of the satellite peaks) in $(GdPd_3)_8Al$ is less than that in $(CePd_3)_8Al_{0.5}Zn_{0.5}$. We found that the intensity of the 'satellite peaks' decreases with the increase of the rare earth atomic number. The lattice parameters of $(RPd_3)_8Al$ and $(CePd_3)_8Zn_{0.5}Al_{0.5}$ are listed in table 1. The values for $(RPd_3)_8Al$ follow the trend expected on the basis of lanthanide contraction.

The thermal variation of the inverse susceptibility, χ^{-1}, between 1.7 and 300 K measured in an applied field of 3–5 kOe of $(RPd_3)_8Al$ compounds is shown in figure 3. A Curie–Weiss behaviour is observed typically between 100 and 300 K in all the compounds. A least squares fitting of the data to the Curie–Weiss expression $\chi = C/(T - \theta_p)$ furnishes the values of the effective paramagnetic moment, μ_{eff}, and the paramagnetic Curie temperature, θ_p, which are listed in table 1. The value of μ_{eff} is nearly the same as the corresponding Hund's rule derived value of the effective magnetic moment of the LS ground multiplet level of the trivalent rare earth ions except for R = Gd, where we found a slight enhancement. To ensure that it is not due to any experimental error, we measured the susceptibility of $(GdPd_3)_8Al$ twice, first in the SQUID and later in the VSM. The two independent sets of data yield the same value of μ_{eff}.

The susceptibility in the low temperature range, measured at various fields for different compounds, is shown in figures 4 and 5. In some cases the susceptibility has been measured

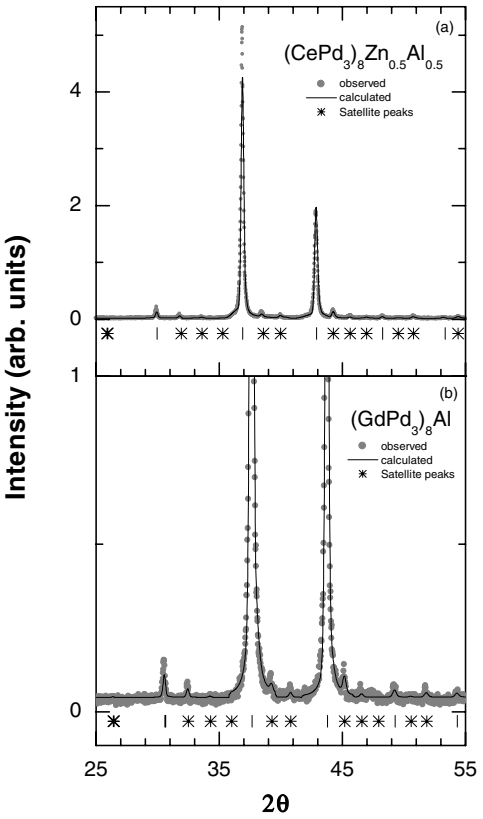

Figure 1. The x-ray diffraction pattern and Rietveld fitting for (a) $(CePd_3)_8Zn_{0.5}Al_{0.5}$ and (b) $(GdPd_3)_8Al$.

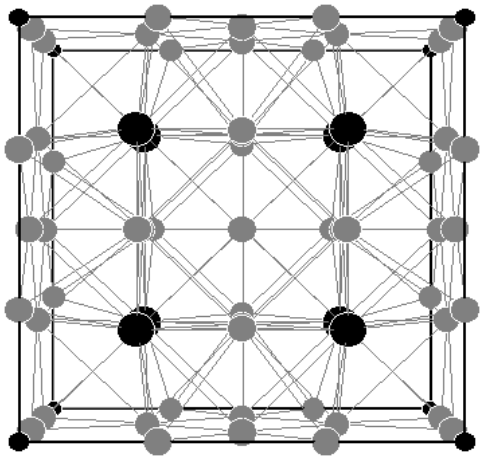

Figure 2. The unit cell of $(RPd_3)_8Al$ showing distortion of the Pd polyhedra: Ce (●); Pd (◯); Al (•).

in both zero-field-cooled (ZFC) and field-cooled (FC) conditions. Peaks in the ZFC data, characteristic of antiferromagnetic transitions, are seen in compounds with R = Gd, Tb, Ho and Dy. It may be noticed that for R = Tb, Dy and Ho the ZFC and FC data differ appreciably below the peak temperature T_N, particularly for Tb and Dy. Similar behaviour was seen earlier in $(TbPd_3)_8T$ (T = Ga and Ge) [10]. We found that the thermomagnetic irreversibility in the Tb compound diminishes with the increase in the applied magnetic field, the irreversibility in 100 Oe being less than that in 50 Oe (figure 4(a)) and nearly vanishing in applied magnetic field of 10 kOe (figure 4(b)). T_N shifts towards low temperatures with increasing magnetic field and in a field of 30 kOe we do not see any peak down to 2 K in $(TbPd_3)_8Al$ (figure 4(b)). Similar behaviour is seen for $(DyPd_3)_8Al$ (figure 5(a)). $(HoPd_3)_8Al$ also exhibits irreversibility in the magnetization below T_N, though somewhat less pronounced compared to the Tb and Dy compounds (figure 5(b)). On the other hand, in $(GdPd_3)_8Al$ the magnetic susceptibility measured in a field of 100 Oe does not show any thermomagnetic irreversibility (figure 5(b)). The ac susceptibility (ac χ) measurements were performed on $(TbPd_3)_8Al$ at frequencies between 1 and 999 Hz; the ac χ data are shown in figure 4(c).

The isothermal magnetization $[M(H)]_T$ of $(RPd_3)_8Al$ measured at various temperatures and up to a field of 60 kOe is shown in figure 6. For $(GdPd_3)_8Al$ we found that $[M(H)]_T$ is linear at 2 and 5 K up to an applied field of 60 kOe and the magnetization at the two temperatures

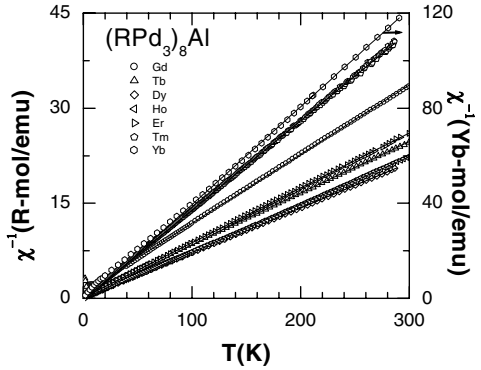

Figure 3. The thermal variation of the inverse magnetic susceptibility of $(RPd_3)_8Al$ compounds. The solid line for each compound is a linear (Curie–Weiss) fit to the data above 100 K.

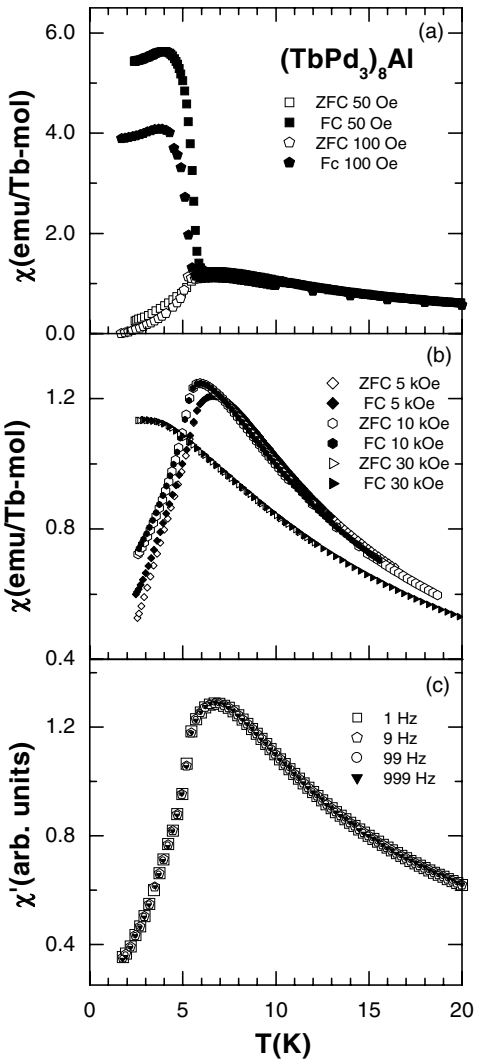

Figure 4. The zero-field-cooled and field-cooled magnetic susceptibility as a function of temperature of $(TbPd_3)_8Al$ (a) in 50 and 100 Oe and (b) in 5, 10 and 30 kOe and (c) ac magnetic susceptibility at 1, 9, 99 and 999 Hz.

is nearly the same (figure 6(a)). In $(TbPd_3)_8Al$, $[M(H)]_{T=1.7\ K}$ exhibits two metamagnetic transitions seen as peaks in the $d[M(H)]_T/dH$ plots and attains a value of about 7.5 μ_B in 60 kOe (figure 6(b)). In the paramagnetic regime at 6 and 10 K the metamagnetic transitions have vanished and at 35 K, far above T_N, the magnetization varies linearly with the field (figure 6(b)). For the sake of comparison we measured $[M(H)]_{T=1.7\ K}$ of $TbPd_3$. There is no metamagnetic transition in the magnetization of $TbPd_3$, though initially it builds up more rapidly than in $(TbPd_3)_8Al$, attaining about 65% of 7 μ_B (M in 60 kOe) in a field of 10 kOe (figure 6(b)). In $(DyPd_3)_8Al$, $[M(H)]_{T=2.7\ K}$ exhibits a sharp metamagnetic transition in a field of 4 kOe and attains a value of 7.5 μ_B in 60 kOe (figure 6(c)). At 3.7 K the metamagnetic

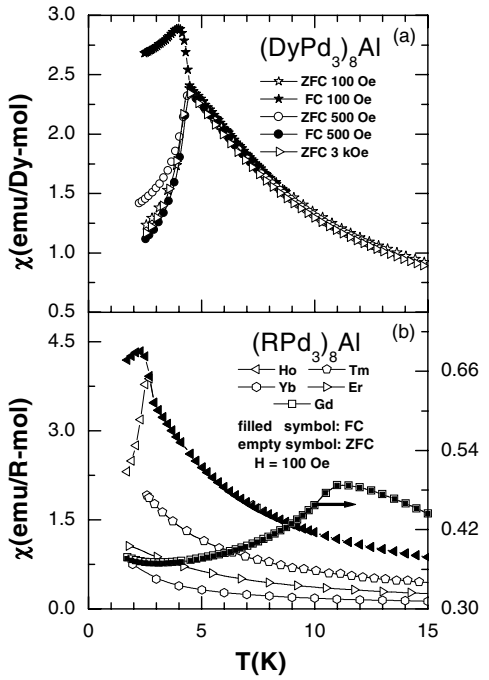

Figure 5. The zero-field-cooled and field-cooled magnetic susceptibility as a function of temperature for (a) $(DyPd_3)_8Al$ in 100, 500 Oe and 3 kOe and (b) $(RPd_3)_8Al$ (R = Gd, Ho, Er, Tm and Yb) in 100 Oe.

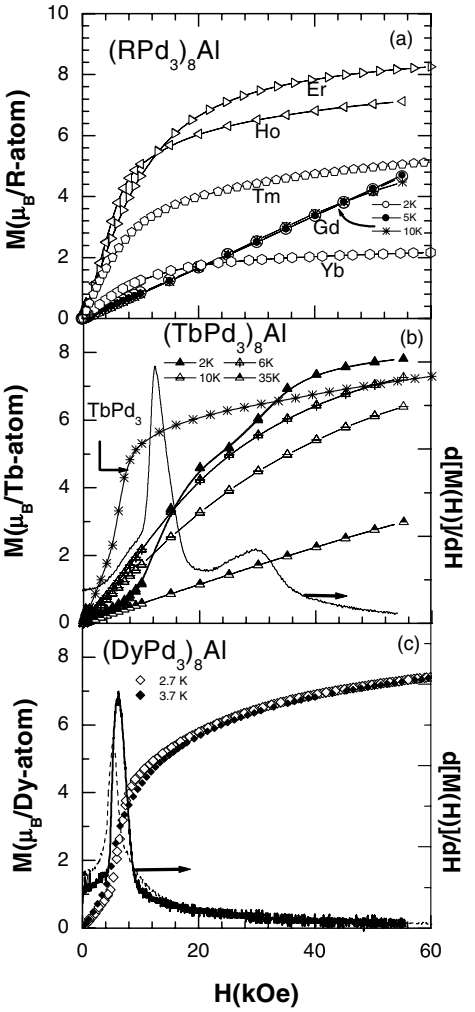

Figure 6. The isothermal magnetization as a function of applied magnetic field for $(RPd_3)_8Al$, (a) R = Ho, Er, Tm and Yb at 2 K and R = Gd at 2, 5 and 10 K; (b) R = Tb at 2, 6, 10 and 35 K; the derivative with respect to the field at 2 K and isothermal magnetization of $TbPd_3$ at 2 K; (c) R = Dy at 2.7 and 3.7 K; also shown are the derivatives at these temperatures.

transition occurs in a lower field, as seen from the shift in the peak of the derivative towards lower field, and the magnetization crosses over the 2.7 K plot at 7 kOe, merging with the latter at higher fields (figure 6(c)). In $(HoPd_3)_8Al$, $[M(H)]_{T=1.7\ K}$ increases rapidly till 10 kOe and less gradually thereafter, attaining a value of 7.2 μ_B in 60 kOe (figure 6(a)). For Er, Tm and Yb $[M(H)]_{T=2\ K}$ is shown in figure 6(a). The data bear qualitative similarity to the data for Tb taken at temperatures above but close to the transition temperatures.

The electrical resistivity of $(RPd_3)_8Al$ compounds is plotted in figure 7. At high temperatures the behaviour is typical of metallic samples with the resistivity varying nearly linearly with temperature. The low temperature resistivity for R = Gd, Tb, Dy and Ho, shown

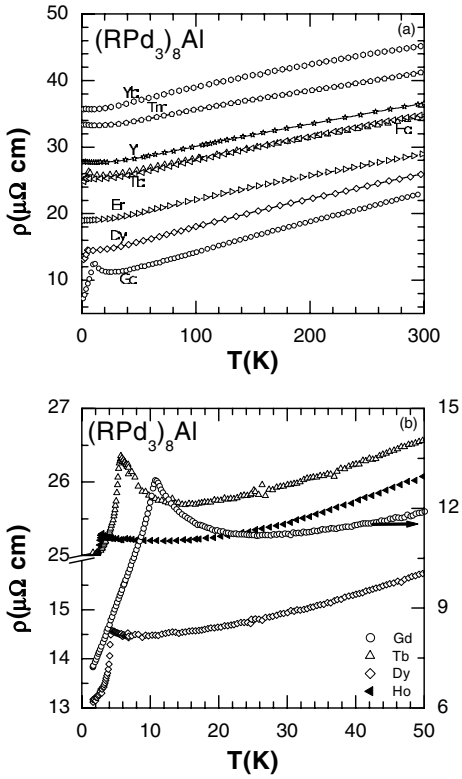

Figure 7. The thermal variation of resistivity of $(RPd_3)_8Al$: (a) R = Gd, Tb, Y, Dy, Ho, Er, Tm and Yb; (b) an enlarged view of resistivity below 50 K for R = Gd, Tb, Dy and Ho showing the resistivity minima.

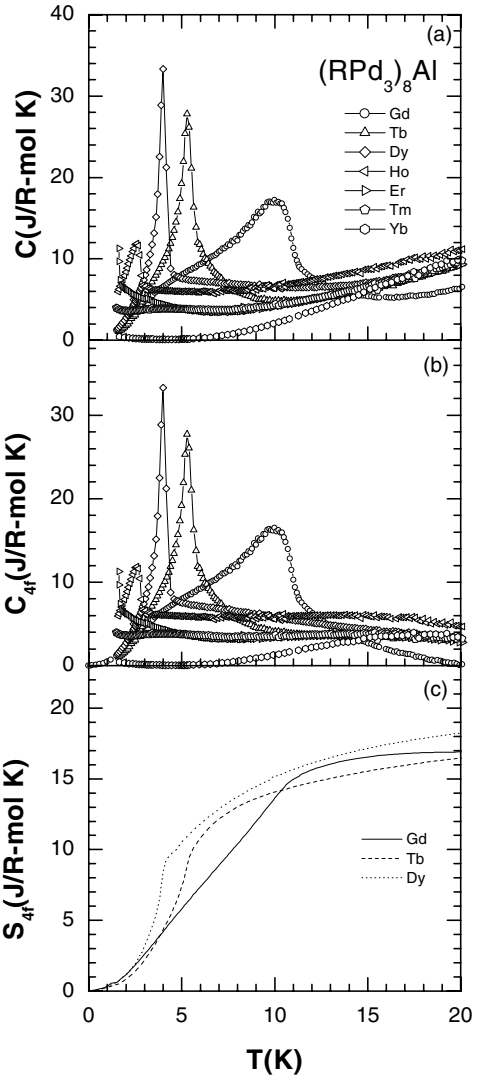

Figure 8. The thermal variation of the heat capacity and entropy of $(RPd_3)_8Al$ (R = Gd, Tb, Dy, Ho, Er, Tm and Yb): (a) total heat capacity; (b) 4f heat capacity; (c) 4f entropy.

in figure 7(b), peaks at temperatures close to the magnetic ordering temperature (T_N) found from the magnetization and the heat capacity data (see below). For $T > T_N$ it exhibits a smooth local minimum at temperatures $\approx 2.5T_N$ and for $T < T_N$ the resistivity decreases monotonically due to the gradual loss of the spin-disorder induced scattering.

The heat capacity, C, data are shown in figure 8(a). For R = Gd, Tb, Dy and Ho the heat capacity exhibits peaks and peak heights, C_{max}, exceed 250 J mol^{-1} K^{-1} in $(TbPd_3)_8Al$ and $(DyPd_3)_8Al$. The peak positions nearly coincide with T_N deduced from the magnetization data and thus the heat capacity confirms the occurrence of long-range magnetic ordering of the rare earth localized magnetic moments in these compounds. For R = Er, the data indicate

that the magnetic order will set in just below $T = 1.6$ K, the lowest temperature attainable in our set-up. $(TmPd_3)_8Al$ and $(YbPd_3)_8Al$ also order below 1.6 K as indicated by the beginning of an upturn in the heat capacity, precursory to the magnetic transition at lower temperatures. For the non-magnetic analogue $(LaPd_3)_8Al$, the magnetic contribution is absent and the heat capacity increases monotonically with the increase in temperature due to the contributions from the phonons and the conduction electrons. The value of the Sommerfeld co-efficient γ, found from the least squares fitting of the data to the expression $C = \gamma T + \beta T^3$ below 6 K, is 0.7 mJ/g atom K^2, which is comparable to the typical values of γ of s–p metals.

Making the usual assumption that the phonon heat capacity of $(RPd_3)_8Al$ compounds with magnetic R is equal to that of the non-magnetic iso-structural analogue $(LaPd_3)_8Al$, we have calculated C_{4f}, the contribution to the heat capacity due to the 4f electrons. C_{4f} is obtained by subtracting the heat capacity of the $(LaPd_3)_8Al$ from the given $(RPd_3)_8Al$, the former properly scaled to take into account the slight difference in the atomic masses of heavy R ions and La. We have also calculated the entropy S_{4f} up to 20 K using the expression

$$S_{4f}(T_0) = \int_0^{T_0} \frac{C_{4f}}{T}\,\mathrm{d}T.$$

For $(GdPd_3)_8Al$ the entropy nearly saturates to 17 J/Gd mol K at 20 K, which is close to the theoretical value of 17.28 J/Gd mol K ($R \ln 8$; $J = 7/2$ for Gd). The entropy in $(TbPd_3)_8Al$ and $(DyPd_3)_8Al$ at 20 K is of similar magnitude but unlike that of Gd it is increasing with temperature.

3.2. $(CePd)_{38}Zn_{0.5}Al_{0.5}$

The heat capacity of $(CePd_3)_8Zn_{0.5}Al_{0.5}$ and the parent $(CePd_3)_8Al$ is shown in figure 9. Both compounds order magnetically as inferred from the peak in the heat capacity with peak height, C_{max}, exceeding 5 J/Ce mol K. For the Zn-substituted compound the peak at 4.6 K occurs about 0.2 K above that of $(CePd_3)_8Al$, showing that Zn substitution of Al by as much as 50% has only a marginal effect on the transition temperature. Compared to [4] the T_N of our sample of $(CePd_3)_8Al$ is higher by 0.6 K. Figure 9 also shows C_{4f} derived by subtracting the heat capacity of the non-magnetic reference compound $(LaPd_3)_8Al$ from the two Ce compounds and the entropy S_{4f}. C_{4f} is sizeable above the magnetic transition suggesting the presence of a Schottky contribution to the heat capacity in the two compounds and possible short-range order. At the transition temperature the entropy is less than $R \ln 2$ (5.76 J/Ce mol K) of a doublet, $S = \frac{1}{2}$ state, and attains the theoretical value at around 10 K. The magnetic ordering in $(CePd_3)_8Zn_{0.5}Al_{0.5}$ is antiferromagnetic as inferred from the peak in the magnetization near 4.6 K, shown in the lower inset of figure 10 and the behaviour of magnetization in applied field below T_N (upper inset figure 10). The inverse susceptibility shows Curie–Weiss behaviour and the least squares fitting of the data between 100 and 300 K to the Curie–Weiss expression for the susceptibility gives $\mu_{eff} = 2.56\ \mu_B\ Ce^{-1}$ and $\theta_p = -30$ K. For $(CePd_3)_8Al$ the corresponding values are $2.42\ \mu_B\ Ce^{-1}$ and -11 K [4]. θ_p has increased by nearly three times in the Zn-substituted compound though T_N values are comparable. Zn substitution brings about some qualitative changes in the thermal variation of the total resistivity as shown in figure 11. In contrast to $(CePd_3)_8Al$, ρ_{total} in the Zn compound decreases with temperature down to 160 K and shows a negative $\mathrm{d}\rho/\mathrm{d}T$ from 160 K down to a broad peak at 50 K. However, $\mathrm{d}(\rho_{4f=\rho Ce} - \rho_{La})/\mathrm{d}T$ is negative in both compounds below 300 K down to their respective peak temperatures.

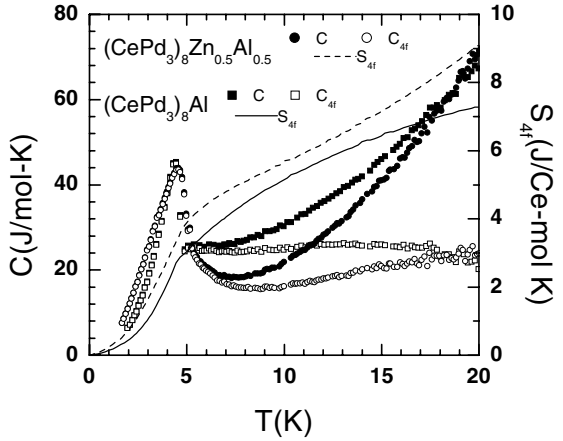

Figure 9. The thermal variation of the total and 4f heat capacity and entropy of $(CePd_3)_8Zn_{0.5}Al_{0.5}$ and $(CePd_3)_8Al$.

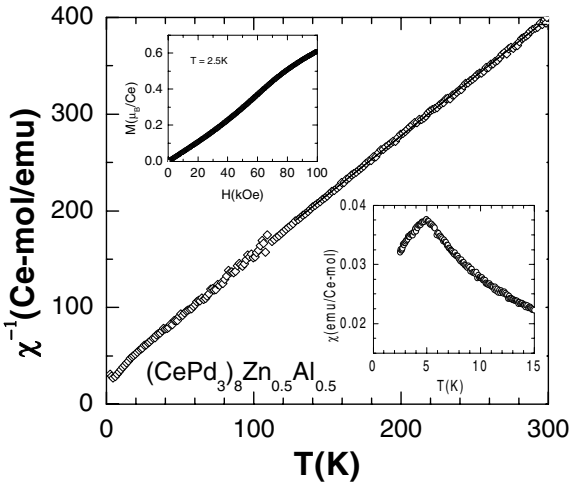

Figure 10. The inverse magnetic susceptibility plotted as a function of temperature for $(CePd_3)_8Zn_{0.5}Al_{0.5}$. Upper inset, field variation of the magnetization at 2.5 K; lower inset, molar susceptibility of $(CePd_3)_8Zn_{0.5}Al_{0.5}$ below 15 K.

4. Discussion

4.1. $(RPd_3)_8Al$ (R = La, Gd, Tb, Dy, Ho, Er, Tm, Yb and Y)

In order to understand the structure of $(RPd_3)_8T$ compounds, it is pertinent to mention here that Dhar *et al* [8] had earlier shown that a smaller atom like boron can be alloyed with RPd_3 to form anti-pervoskite interstitial alloys of the formula RPd_3B_x ($0 < x \leqslant 1$), where the boron atom is randomly incorporated in the body-centre position of the RPd_3 unit cell. Alloying with boron led to an expansion of the unit cell. Gordon *et al* [1, 2] found that when the alloying atom T is bigger than boron, it forms a superstructure at the composition $(RPd_3)_8T$ (i.e. at $x = 0.125$). This can be understood by considering a super-cube having three layers stacked

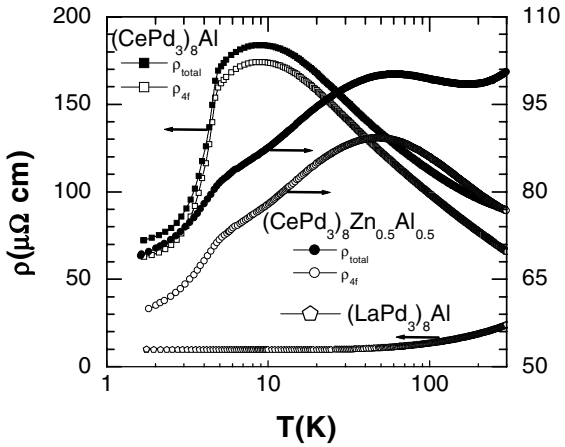

Figure 11. The thermal variation of the total (ρ) and magnetic (ρ_{4f}) resistivity of $(CePd_3)_8Zn_{0.5}Al_{0.5}$, $(CePd_3)_8Al$ and ρ of $(LaPd_3)_8Al$.

one on top of other with nine unit cubes in each layer. Each unit cube in a layer represents the face-centred-cubic unit cell of RPd_3 with R atoms at the vertices and Pd atoms at the face centres of the cube. Thus, there are 27 cubic blocks in the super-cube. The effect of placing T atoms at the body centre position in the eight corner cubes, C_i^t and C_i^b ($i = 1$–4), of top (t) and bottom (b) layers is such that no additional T atoms can be accommodated in the remaining 19 unit cubes. For example, in the top layer the presence of T atoms in C_1^t and C_2^t causes Pd atoms at the faces shared by C_1^t–S_1^t (S_i^t, $i = 1$–4, are the four side cubes in the top layer) and C_2^t–S_1^t to displace by δ_1 towards the centre of S_1^t. This pushes out the Pd atoms at the remaining four faces of S_1^t causing them to move outwards by δ_2 ($\delta_2 < \delta_1$). Similar displacements of Pd atoms occur in the other $S_{i=2,3,4}^t$. As O^t (the central cube in the top layer) shares a face each with each S_i^t, the Pd atoms on each of these four faces have actually displaced by δ_2 towards the centre of O^t. The displacement δ_2 is small compared to δ_1 and therefore has no effect on the remaining two Pd atoms of O^t. Therefore, all the Pd atoms other than the ones on top and bottom faces of O^t have been displaced inwards towards the centre of O^t [1]. The displacements of the Pd atoms off the faces towards the centre of $S_{i=1,2,3,4}^t$ and O^t cells (described above) do not leave enough space around the body-centre positions to be occupied by the big T atom. So, in the top layer of the super-cube once the corner cells are filled with T atoms no further T atom can be added. The top layer of the super-cube, therefore, cannot hold more than four T atoms. The bottom layer behaves identically to the top layer. Turning our attention now to the nine unit cubes in the middle layer (m), the $C_{i=1,2,3,4}^m$ of the middle layer cannot hold a Pd atom at the body-centre position because the $C_{i=1,2,3,4}^{t,b}$ in the adjacent layers are filled. $S_{i=1,2,3,4}^m$ cannot hold a Pd atom either, because the Pd atoms on the S_i^m–$S_i^{t,b}$ interface and S_i^m–C_i^m interface have moved inwards (by δ_2) toward the centre of S_i^m not leaving enough space around the body-centre position of S_i^m for it to be occupied by the big T atom. The Pd atoms on the faces shared by O^m and the S_i^m and on O^m–O^t and O^m–O^b interfaces have not moved from their places. Therefore, in the O^m cell the space around the body-centre position is not squeezed. Despite this its centre is not occupied by a T atom because it will push the Pd atoms in the reverse direction of Pd displacements described above, which will disturb the equilibrium. Therefore, the middle layer stays devoid of any T atom. In a nutshell, if we pick any one RPd_3 unit cell randomly and put a T atom at its body-centre position then

a T atom is denied in all the adjacent cells up to a distance less than or equal to $a\sqrt{3}$, where a is the cell parameter of RPd_3 and the distances are measured between the centres of the unit cells. It is worthwhile to note that the T atom also displaces the eight R atoms outward; thus a cell with a T atom is bigger than the cell without a T atom. The unit cell of $(RPd_3)_8T$ with T atoms at the vertices is shown in figure 2. It should be noted that though the conventional unit cell chosen for $(RPd_3)_8Al$ has the cubic symmetry, the local symmetry around the rare earth ion is lower than cubic due to the introduction of T atoms in the structure and to the small displacements suffered by the Pd atoms thereupon.

The μ_{eff} in the Gd compound is in slight disagreement with the theoretically derived value of 7.94 μ_B for Gd^{3+}. The enhancement of μ_{eff} in the Gd compound may be attributed to conduction electron polarization. The absolute magnitude of θ_p is relatively small in the whole series, having the maximum value of 10 K in $(GdPd_3)_8Al$. Negative values of θ_p are obtained for R = Gd, Dy and Er whereas θ_p is positive for R = Tb, Ho, Tm and Yb. However, low-field measurements show that the compounds order antiferromagnetically. For Tm, Er and Yb the nature of magnetic ordering could not be ascertained as the transition occurs below 1.7 K. A comparison with the magnetic ordering temperatures of the corresponding RPd_3 compounds (see table 1) shows that the formation of superstructure enhances T_N. For the remaining $(RPd_3)_8Al$ compounds with magnetic rare earth ions, the magnetic transitions take place at temperatures below 1.7 K, the lowest temperature attainable in our set-up. In the mean-field approximation [9], the paramagnetic Curie temperature θ_p ($=T_N$) depends upon the average conduction electron to atom ratio, s–f exchange integral J and the RKKY sum $\sum 2k_F r$, k_F being the Fermi wavevector. We believe that the changes in T_N are due to the variation in $\sum 2k_F r$ between the parent RPd_3 and corresponding $(RPd_3)_8Al$.

The huge thermomagnetic irreversibility observed in the susceptibilities of Tb, Dy and Ho cannot be attributed to a spin glass ordering of the rare earth ions, since we see robust and sharp peaks in the heat capacity data at T_N. It should be noted that in spin glasses the field-cooled susceptibility is nearly constant below the freezing temperature and greater than the ZFC susceptibility, unlike the case here where at sufficiently large fields the ZFC and FC susceptibilities coincide. Further evidence against spin-glass-type freezing comes from the ac χ data taken on $(TbPd_3)_8Al$. The peak in the ac χ is frequency independent ruling out spin-glass-type freezing of the Tb ions. It appears that the antiferromagnetic configuration for R = Tb, Dy and Ho is sensitive to the applied field. We do not see any thermomagnetic irreversibility in the low-field susceptibility of the Gd compound. It should be noted that while the orbital angular momentum for the Gd ion is zero, the other R ions possess a sizeable orbital angular momentum and a large spin–orbit coupling, contributing to their total magnetic moment. The orbital contribution is affected by the crystal electric field (CEF) and is responsible for the magnetocrystalline anisotropy. Therefore, a difference in the ZFC and FC magnetization below T_N may be related to the presence of anisotropy in R = Tb, Dy and Ho. It may be mentioned that a small magnetic correlation length can also lead to strong magnetic irreversibility in the antiferromagnetic state. There is a qualitative difference between the isothermal magnetization $[M(H)]_T$ of $(GdPd_3)_8Al$ and $(RPd_3)_8Al$, R = Tb, Dy and Ho measured at various temperatures and up to a field of 60 kOe (figure 6). For Er, Tm and Yb the magnetization data taken at 2 K are qualitatively similar to the data for Tb taken at temperatures above but close to the transition temperatures, implying that these compounds order magnetically below 2 K.

A brief description of the neutron scattering results on RPd_3 (R = Nd, Tb, Dy, Er, Tm and Yb) may be pertinent here [11]. In $TbPd_3$, the data were explained by assuming two incommensurate propagation vectors $\boldsymbol{k}_{\text{Tb}}$ and $\boldsymbol{k}_{\text{Pd}}$ characterized by different critical exponents in the temperature dependence of the corresponding magnetizations. The ordered magnetic

moments of Tb induce a moment on the Pd sub-lattice. A sinusoidal modulation for both Tb and Pd moments (and a distinct possibility of helical arrangement of the Tb sub-lattice) were deduced to be the most likely representation of the magnetic structure in $TbPd_3$. It was observed that weak magnetic fields induce a ferromagnetic component and suppress the induced magnetic ordering of the Pd sub-lattice. The ferromagnetic component was maximum at the critical temperature of the antiferromagnetic ordering, the latter decreasing with increasing applied fields. In $DyPd_3$, the lattice is ferromagnetic at 1.9 K but short-range spin fluctuations with a propagation vector $\boldsymbol{k} = (1/2, 1/2, 0)$ undergo a long-range ordering at low temperatures giving rise to a ferrimagnetic configuration at 0.6 K. Overall, it was found in [11] that the complexity of the long-range magnetic order increases with decreasing $4f^n$ occupancy of the rare earth ions. Since the crystal symmetry of RPd_3 and $(RPd_3)_8Al$ is the same and Al atoms constitute just 3 mol% of $(RPd_3)_8Al$, we believe that the magnetic correlations in $(RPd_3)_8Al$ may retain some characteristics found in the corresponding RPd_3 analogues. A definitive understanding of the details of the magnetic ordering in $(RPd_3)_8Al$ may be obtained from an analogous inelastic neutron scattering study of these ternary compounds.

Shallow resistivity minima are seen for R = Ho, Tm and Yb below 25 K. The minima are more pronounced for R = Tb, Dy and Gd and the minimum occurs at 25 K for R = Gd (figure 7(b)). Since the minima, T_{min}, occur at $T > T_N$, the upturn in the resistivity for $T < T_{min}$ in the paramagnetic regime cannot be attributed to the magnetic-superzone-induced gap effects. As the antiferromagnetic order is associated with large reciprocal magnetic lattice vector, typically for $T > T_N$ the large-$\boldsymbol{k}$ (where $\boldsymbol{k}$ is the wavevector) fluctuations diminish while small-$\boldsymbol{k}$ fluctuations grow [12], which should lead to a decreasing resistivity in antiferromagnetic metals above T_N. The overall details of the Fermi surface and the magnetic structure may, however, bring qualitative changes in the thermal variation of the resistivity above T_N. The minima in the resistivity arise because the phonon contribution to the resistivity is increasing slower than the decrease of the critical resistivity in the paramagnetic region, resulting in a negative temperature coefficient for the resistivity in a certain range of temperature. Similar variations of resistivity have long been seen in rare earth metals, Eu and Tb, for example. The T_N and T_{min} of Eu is 89 and 145 K respectively and the corresponding temperatures for Tb are 145 and 265 K respectively. The role of critical scattering in the resistivities of Eu, Tb and other rare earth metals has been pointed out by Meaden *et al* [13].

The occurrences of sharp and huge peaks in the heat capacity data for R = Gd, Tb, Dy and Ho at temperature close to the magnetic ordering temperature as deduced from the low-field-susceptibility and resistivity measurements confirm the long-range magnetic ordering in these compounds. Assuming that the heat capacity due to the conduction electrons is the same in all the compounds, then the C_{4f} will consist of the magnetic heat capacity due to the magnetic ordering of the rare earth magnetic moments and the Schottky heat capacity arising from the thermal variation of the fractional occupation of CEF split levels. The thermal variation of C_{4f} is shown in figure 8(b). It may be noted that C_{4f} becomes negligible at around 20 K ($\sim 2T_N$) only for $(GdPd_3)_8Al$, whereas for other compounds, even though they have a lower T_N compared to the Gd analogue, C_{4f} is appreciable even at 20 K. Further broad peaks in C_{4f} occur for R = Er, Yb and Tm and both these effects can be attributed to the Schottky heat capacity. The CEF splitting in some RPd_3 compounds has been measured by inelastic neutron scattering and the first two excited states are spaced at 4 and 20.7 K in $ErPd_3$, 20.6 and 32.9 K in $DyPd_3$ and 4.9 and 25.2 K in $TmPd_3$ [14]. In $YbPd_3$ the first excited state is at 47 K. If the CEF splitting in $(RPd_3)_8Al$ compounds is comparable to that in the corresponding RPd_3 analogues then there will be significant Schottky heat capacity below 20 K as suggested by the data. Since Gd is an S-state ion, the CEF effects are negligible.

4.2. $(CePd_3)_8Zn_{0.5}Al_{0.5}$

It is seen that while $(CePd_3)_8T$ compounds with T in the group 13 p-block elements show features that can be assigned to strong Kondo interactions, those with T in the group 14 p-block elements show normal metallic behaviour [4]. The electrical resistivity of $(CePd_3)_8Al$, for example, shows a negative $d\rho/dT$ from 300 K down to the peak at 14 K [4]. The peak is probably due to the coherence effects in a dense Kondo lattice as the compound orders magnetically at a much lower temperature of 3.8 K. With the group 12 element Zn, Jones *et al* [4] did not get a homogeneous end product. We, therefore, tried substituting Zn for Al and we find that $(CePd_3)_8Zn_{0.5}Al_{0.5}$ is single phase with lattice parameter slightly larger than that of $(CePd_3)_8Al$. Our primary motivation was to find how the magnetic exchange and Kondo interactions are affected with Zn substitution.

The magnetic ordering temperature due to the Zn substitution has changed only marginally. An estimation of the magnitude of the entropy indicates that the CEF ground state is most probably a doublet. Typically in a magnetic transition the entropy associated with the magnetic ordering of the spins is fully released some degrees above the transition temperature due to the invariable presence of the short-range order. If the Kondo interaction is present the spin may partially be quenched leading to reduced entropy associated with the magnetic ordering.

The rapid fall in the resistivity below 50 K in $(CePd_3)_8Zn_{0.5}Al_{0.5}$ arises due to the coherence effects in a dense Kondo lattice similar to that in the parent compound. The resistivity decreases when the temperature is smaller than the CEF splitting as the degeneracy of the 4f level decreases [15]. The change in the fractional occupation of the CEF levels with temperature will also vary the Kondo temperature as the latter depends on the degeneracy of the 4f level. Therefore, the thermal variations of the resistivities in $(CePd_3)_8Al$ and the Zn-substituted compounds, arising from an interplay of CEF splitting and the Kondo effect, suggest that the Kondo temperature in the high-temperature regime may be different in the two compounds. That may also partially account for the larger-θ_p in the Zn-substituted compound deduced from the magnetization data, as the presence of Kondo interaction is believed to contribute a negative θ_p in the Curie–Weiss expression for the susceptibility. The change in the slope of resistivity at T_N (indicated in the figure) is due to the magnetic transition as the spin scattering gradually freezes out.

5. Conclusion

To conclude, we have synthesized new compounds of formula $(RPd_3)_8Al$ for various *R* and $(CePd_3)_8Zn_{0.5}Al_{0.5}$. Their magnetic, transport and thermodynamic properties have been studied. The compounds of the series $(RPd_3)_8Al$ obey the de Gennes scaling with the exception of the Ce compound, which orders at an anomalous high temperature of 4.4 K. Interesting thermomagnetic irreversibility in the magnetic susceptibilities below T_N is seen for R = Tb, Dy and Ho, which is absent in the Gd analogue. Neutron inelastic scattering on these compounds should provide further insight into their magnetic behaviour.

References

[1] Gordon R A and DiSalvo F J 1996 *Z. Naturf.* B **51** 52
[2] Gordon R A, Jones C D W, Alexander M G and DiSalvo F J 1996 *Physica* B **225** 23
[3] Mitra C, Dhar S K and Ramakrishnan S 1999 *Solid State Commun.* **110** 701
[4] Jones C D W, Gordon R A, Cho B K, DiSalvo F J, Kim J S and Stewart G R 1999 *Physica* B **262** 284
[5] Cho B K, Gordon R A, Jones C D W, DiSalvo F J, Kim J S and Stewart G R 1998 *Phys. Rev.* B **57** 15191
[6] Mitra C, Dhar S K, Ramakrishnan S and Patil N G 1999 *Physica* B **259–261** 108

[7] Mitra C, Dhar S K and Ramakrishnan S 2000 *J. Appl. Phys.* **87** 5146
[8] Dhar S K, Malik S K and Vijayaraghavan R 1981 *Mater. Res. Bull.* **16** 1557
[9] de Gennes P G 1962 *J. Physique Radium* **23** 510
[10] Mitra C 2001 *PhD Thesis* Mumbai University
[11] Elsenhans O, Fischer P, Furrer A, Clausen K N, Purwins H G and Hulliger F 1991 *Z. Phys.* B **82** 61
[12] Balberg I 1977 *Physica* B **91** 71
[13] Meaden G T, Sze N H and Johnston J R 1972 *Dynamical Aspects of Critical Phenomena* ed J I Budnik and M P Kawatra (New York: Gordon and Breach) p 315
[14] Elsenhans O, Furrer A, Purwins H G and Hulliger F 1990 *Z. Phys.* B **80** 281
[15] Cornut B and Coqblin B 1972 *Phys. Rev.* B **5** 4541
[16] Gardner W E, Panfold J, Smith T F and Harris I R 1972 *J. Phys. F: Met. Phys.* **2** 133